Intermetallics 93 (2018) 235–243

Contents lists available at ScienceDirect

Intermetallics

journal homepage: www.elsevier.com/locate/intermet

Exploring thermoelectric materials for renewable energy applications: The case of highly mismatched alloys based on $AlBi_{1-x}Sb_x$ and $InBi_{1-x}Sb_x$

Bakhtiar Ul Haq[a,*], R. Ahmed[b,c], S. AlFaify[a,**], Faheem K. Butt[d,e], A. Shaari[b], A. Laref[f]

[a] Advanced Functional Materials & Optoelectronics Laboratory (AFMOL), Department of Physics, Faculty of Science, King Khalid University, P.O. Box 9004, Abha, Saudi Arabia
[b] Department of Physics, Faculty of Science, Universiti Teknologi Malaysia, UTM Skudai, 81310 Johor, Malaysia
[c] Center for High Energy Physics, University of the Punjab, Quid-e-Azam Campus Lahore, 54590 Pakistan
[d] Division of Science and Technology, University of Education, College Road, Township, Lahore, Pakistan
[e] Physik Department, Chair of Energy Conversion and Storage, Technische Universität München, Garching, Germany
[f] Department of Physics and Astronomy, College of Science, King Saud University, Riyadh, 11451 Saudi Arabia

A B S T R A C T

The high throughput thermoelectric devices are considered promising futuristic energy source to control global warming and realize the dream of green energy and sustainable environment. The ability of the highly mismatched alloys (HMAs), to show the intriguing impact on the physical properties with controlled modifications, has extended their promise to thermoelectric applications. Here, we examine comprehensively the potential of the two prototypical HMAs such as $AlBi_{1-x}Sb_x$ and $InBi_{1-x}Sb_x$ for thermoelectric applications within density functional theory together with the Boltzmann transport theory. For comprehensive understanding, alloying of these materials has been performed over the entire composition range. From our calculations, we found, the replacement of Sb with Bi leads to a significant evolution in the energy band-gap and effective masses of the charge carriers that consequently deliver enhancement in thermoelectric response. Improvement of magnitude 1.25 eV and 0.986 eV has been respectively recorded in band-gaps of $AlBi_{1-x}Sb_x$ and $InBi_{1-x}Sb_x$ for the **across** composition alloying. Similarly, by the electronic-structure engineering of HMAs, thermoelectric properties such as, the Seebeck coefficients over Fermi-level were found to be improved from 82.90 μV/K to 107.52 μV/K for $AlBi_{1-x}Sb_x$ and 60.32 μV/K to 92.73 μV/K for $InBi_{1-x}Sb_x$. As a result, the thermoelectric figure of merit (ZT) and power factor show considerable enhancement as a function of alloying composition for both alloys at room temperature. However, at a higher temperature, the thermal conductivity of these materials experience an exponential increase, results in lower ZT values. Overall, the observed evolution in the electronic structure and thermoelectric response for replacing Sb over Bi is significant in $AlBi_{1-x}Sb_x$ as compared to $InBi_{1-x}Sb_x$. Hence, with the capability of significant and controlled evolution in electronic-structure and subsequent thermoelectric properties, HMAs particularly $AlBi_{1-x}Sb_x$ are believed potential candidates for thermoelectric applications.

1. Introduction

Developing high-performance thermoelectric devices is considered as an alternative source of sustainable energy and is expected to play a key role in reducing environmental pollution. The unique potential of the thermoelectric devices to convert waste heat into electrical energy for power generation and refrigeration shows great promise to realize a dream of low-carbon society. Moreover, thermoelectric devices are also believed to be highly reliable, vibration and noise-free source of energy. It is from this perspective; research on the high-throughput thermoelectric materials is underway from the past few years [1–3].

The performance of a thermoelectrics is evaluated by its dimensionless parameter called the figure of merit (ZT) as a primary metric. The relatively small ZT value of the currently established thermoelectric materials is a bottleneck for their applications as power generators and cooling devices. The ZT value is determined by the interrelated physical parameters such as Seebeck coefficient (S) also known as thermopower, the electrical conductivity, and thermal conductivity using the following mathematical expression:

$$ZT = \frac{S^2 \sigma T}{\kappa} \quad (1)$$

* Corresponding author.
** Corresponding author.
E-mail addresses: bakhtiarjadoon@gmail.com (B. Ul Haq), sasaalfaify@hotmail.com (S. AlFaify).

http://dx.doi.org/10.1016/j.intermet.2017.09.017
Received 14 July 2017; Received in revised form 25 September 2017; Accepted 25 September 2017
Available online 08 November 2017
0966-9795/

Thus the improvement in ZT can be realized on account of the large value of Seebeck coefficient, high electrical conductivity, and small thermal conductivity. In principle, the ideal value of ZT cannot be obtained due to the inherent conflict among these material's properties. For instance, larger Seebeck coefficient value can be obtained for low carrier concentration that leads to lower electrical conductivity, while high electrical conductivity is accompanied by larger thermal conductivity [4]. Ultimately, the tradeoff among these parameters can be circumvented by optimizing a number of fundamental parameters such as the effective mass of the charge carriers, carrier concentration, and the electronic and lattice thermal conductivities [5]. Therefore, various approaches including surface roughening [6], nanostructuring [7,8], or alloying [9,10], have been realized in literature to improve the thermal efficiency of thermoelectric materials in terms of optimized ZT value.

Among the aforesaid methods, alloying is a simpler, more straightforward as well as promising avenue for engineering efficient thermoelectric materials due to its capability to bring controlled modifications in the physical properties of materials as a function of alloying composition. The composition induced controlled modification of the physical properties is, however, more prominent in a class of alloys named highly mismatched alloys (HMAs).

HMAs are realized by replacing the anions of the host matrix with iso-valent constituents having distinctly mismatched ionic radii and electronegativity values. Such practice of anion-anion replacement persuades impressive evolution in their electronic band structure and subsequent physical properties. A controlled evolution in the electronic band is therefore expected to deliver enhanced thermoelectric properties of HMAs. It is for this reason, HMAs are expected to be promising materials for applications in high-efficiency thermoelectric devices. However, to our knowledge, limited studies on HMAs such as $ZnSe_{1-x}O_x$ [11], $InP_{1-x}Bi_x$ [12], GaN_xAs_{1-x} [10] and $GaN_{1-x}Sb_x$ [13] are found concerning thermoelectric applications. Furthermore, materials comprising of heavy elements and possessing narrower bandgap are reported to exhibit a low frequency of vibration, resulting in low lattice thermal conductivity [14,15]. Therefore, the realization of the high value of the figure of merit and efficiency from the designing of HMAs comprised of heavy elements is expected. Besides, comprehensive understanding of the nature of the modification in the band-structure and its subsequent effects on the thermoelectric properties of the HMAs within the atomic-scale electronic structure is also rarely analyzed. Having established that HMAs with heavy constituents are capable of the large thermoelectric figure of merit, it is, therefore, instructive to explore the subsequent effects of evolution in the electronic structure on their thermoelectric properties on account of the alloying composition. The first-principles electronic structure calculations combined with the Boltzmann transport theory is considered suitable approach and has been applied successfully to design/discover potential thermoelectric materials, as well as to predict optimum doping level in established thermoelectric materials [5,16–18].

In this paper, we explore the thermoelectric properties of two prototypical HMAs with heavy elemental constituents such as $AlBi_{1-x}Sb_x$ and $InBi_{1-x}Sb_x$ using DFT coupled with semiclassical Boltzmann theory. Calculations concerning electronic band structures are performed using full-potential linearized-augmented-plus-local-orbital (FP-L(APW + *lo*)). The modified Becke-Johnson (mBJ) has been used for treating the exchange part of the exchange-correlation energy, whereas, for the correlation part, the generalized gradient approximations parameterized by Perdew et al. (PBE-GGA) has been used. The calculations for thermoelectric properties have been performed on the top of electronic structure calculations using the semiclassical Boltzmann theory in the BoltzTraP code. For a comprehensive understanding of the effect of composition on the properties of these materials, alloying has been done **across** the entire compositional range such as $x = 0$, 0.25, 0.50, 0.75, and 1. Furthermore, the dependence of thermoelectric response of the $AlBi_{1-x}Sb_x$ and $InBi_{1-x}Sb_x$ on the temperature and chemical potential has been provided in details.

To our knowledge, this study is new of its kind and is therefore believed to provide an opportunity for the use HMAs based on $AlBi_{1-x}Sb_x$ and $InBi_{1-x}Sb_x$ as prosperous thermoelectric material.

1.1. Computational details

Different compositions of $AlBi_{1-x}Sb_x$ and $InBi_{1-x}Sb_x$ for $x = 0$, 0.25, 0.50 0.75 and 1 are realized by the systematic replacement of anions in a simple supercell containing eight atoms. The literature demonstrates this scheme of alloying **across** entire composition as an established approach for designing various highly ordered alloys including HMAs with satisfactory results. Some prominent examples of such alloys are $Be_xZn_{1-x}Te$ [19], $Si_{1-x}Ge_x$ [20], $Ga_{1-x}In_xN$ [21], $GaAs_{1-x}Bi_x$ [22,23], and $Al_{1-x}Tl_xN$ [24], etc. The present investigations of composition induced modifications in the electronic structure and thermoelectric properties are started with calculations for band structure with DFT based FP-L(APW + *lo*) method. Within this method, the basis set is accomplished by the division of the unit cell into non-overlapping spheres around the atoms and the interstitial region. The wave functions are represented differently in both regions, such as atomic-like wave function in the spherical region whereas plane wave basis set in the interstitial region. In spherical region (muffin-tin spheres), wavefunctions have been expanded up to $l_{max} = 10$, whereas energy cutoff $K_{max} = 8.0/R_{MT}$ (Ryd) $^{1/2}$ has been taken into account for the convergence of eigenvalues in the interstitial region. The mBJ exchange potential [25–27] together with PBE-GGA [28] has been used respectively for the treatment of exchange and correlation parts of exchange-correlation energy. The spin-orbit coupling (SOC) has been included to the mBJ potential (mBJ + SOC) through the second variational procedure [29,30]. The geometry optimization has been carried out by relaxing the ionic positions and cell size so that to realize the ground state. The reduced muffin-tin values for Al, In, Sb and Bi are chosen as 2.08 a. u, 2.34 a. u, 2.42 a. u, and 2.46 a. u respectively. The Fourier-expanded charge density was truncated at $G_{max} = 16$ au^{-1}. The Monkhorst–Pack special k-points approach [31] has been adapted for the integration of the Brillion Zone (BZ). The integrals over the special BZ are performed up to 500 (10 × 10 × 10) k-points for good convergence of energy. The total energy was converged up to 10^{-5}Ryd/unit cell in the present self-consistent computations for well-defined results. The electronic structure related calculations with the provided computational details have executed by WIEN2k code [32].

The calculations for thermoelectric properties have been performed within a semiclassical Boltzmann theory under a constant scattering time approximation as implemented in the BoltzTraP code [33]. The details of Boltzmann transport theory are available in Refs. [16,34]. However, we provide a brief summary of the present thermoelectric calculations in the following as well.

The major thermoelectric parameters such as electrical conductivity ($\sigma_{\alpha\beta}$), Seebeck coefficient ($S_{\alpha\beta}$) and power factor are determined as a function of temperature (T) and chemical potential (μ) by using the following equations.

$$\sigma_{\alpha\beta}(T,\mu) = \frac{1}{\Omega}\int\sum_{\alpha\beta}(\varepsilon)\left[-\frac{\partial f_0(T,\ \varepsilon,\ \mu)}{\partial\varepsilon}\right]d\varepsilon, \tag{2}$$

$$S_{\alpha\beta}(T,\mu) = \frac{1}{eT\Omega\sigma_{\alpha\beta}(T,\mu)}\int(\varepsilon-\mu)\Sigma_{\alpha\beta}(\varepsilon)\left[-\frac{\partial f_0(T,\ \varepsilon,\ \mu)}{\partial\varepsilon}\right]d\varepsilon, \tag{3}$$

Where α and β are Cartesian indices of the tensor quantities. Symbols e, Ω and f_o represent the electronic charge, volume of the unit cell and the Fermi–Dirac distribution function of the carriers respectively.

The energy projected transport distribution function represented by $\Sigma_{\alpha\beta}$ is the central term in equations (1) and (2) and can be defined as

$$\Sigma_{\alpha\beta}(\varepsilon) = \frac{e^2}{N}\sum_{i,k}\tau v_\alpha(i,k)v_\beta(i,k)\delta(\varepsilon-\varepsilon_{i,k}), \quad (4)$$

where $v_\alpha(i,k) = \frac{1}{\hbar}\frac{\partial\varepsilon_{i,k}}{\partial k_\alpha}$ represents the group velocity.

In Eq. (3), i, k, N, and τ are used for the band index, wave vector, the total number of k-points used in sampling the BZ, and the relaxation time, respectively. Since the wave-vector-dependent relaxation time is an undetermined quantity in the present calculations, the τ-dependent quantities such as electrical conductivity and power factor are reported with respect to τ i.e σ/τ and $S^2\sigma/\tau$.

2. Results and discussion

Literature shows that first-principles calculations based on the conventional local density approximations and/or generalized gradient approximations typically lead to disagreement with experimental results particularly those associated with the electronic structure. The addition of mBJ exchange potential is however established to reproduce the band structure/band gap as factual as GW approximation [26,35–38]. Furthermore, the thermoelectric properties within Boltzmann transport theory are governed by electronic structure results as preliminary inputs. Therefore, the proper description of the electronic structure is necessary in order to obtain precise results for thermoelectric coefficients. Using electronic structure data obtained with mBJ potential as input for thermoelectric calculations is therefore believed to reproduce sufficiently accurate results for thermoelectric properties.

Fig. 1, shows the energy band structures of $AlBi_{1-x}Sb_x$ and $InBi_{1-x}Sb_x$ determined using mBJ + SOC in the energy span ± 4 eV relative to Fermi level. We found a trivial difference in the electronic band structures determined with and without SOC. As an example, the electronic band structure of $AlBi_{0.75}Sb_{0.25}$ determined with mBJ and mBJ + SOC has been provided in the supplementary file (S1). It is found that SOC leads a minor splitting of bands in the lower part of valence band or in the upper conduction band whereas the valence band maximum (VBM) and conduction band minimum (CBM) remain unchanged. We, therefore, believe that the SOC has a negligible effect on our results. In Fig. 1, one can see that the composition of Sb significantly altered the band structures of $AlBi_{1-x}Sb_x$ and $InBi_{1-x}Sb_x$ both in the arrangement of bands and energy gaps. It is seen from Fig. 1 that AlBi, $AlBi_{0.75}Sb_{0.25}$, $AlBi_{0.50}Sb_{0.50}$ and $AlBi_{0.25}Sb_{0.75}$ exhibit direct band gap as their VBM and CBM occur simultaneously at high symmetry Γ-point in BZ. However, the CBM appears along Γ–X direction in the case of AlSb reflecting its indirect bandgap nature which is also reported in Ref. [39]. Unlike $AlBi_{1-x}Sb_x$, the band-gap of $InBi_{1-x}Sb_x$ is of the direct nature of all the investigated compositions with their VBM and CBM at same Γ-point in the BZ. However, the modifications in the electronic band structures of $InBi_{1-x}Sb_x$ are marginal as compared to $AlBi_{1-x}Sb_x$. To realize the contribution of various electronic states to the observed modifications in the electronic structures on account of compositional change, we determined the orbital resolved band structures (provided in the supplementary file S1). The orbital resolved electronic band structures show that electronic properties of $AlBi_{1-x}Sb_x$ and $InBi_{1-x}Sb_x$ are majorly defined by the *s, p* electrons associated with Al, In, Bi and Sb. The bands formed by these electrons are majorly localized either in the upper valence band or in the lower conduction band. The lower part of the conduction bands is contributed mainly by the *s*-electrons whereas the *p*-electrons are found to be localized in the upper part of the valence bands. The conduction band minima of $AlBi_{1-x}Sb_x$ and $InBi_{1-x}Sb_x$ are defined by hybridized Al-*s*, Bi-*s* and Sb-*s* states. These states are found peculiarly susceptible for the alloying composition. The role of *d*-electrons associated to In, Bi, and Sb are nevertheless insignificant to the electronic properties of the investigated alloys.

The band-gaps of the investigated alloys experience linear increase with an increase in Sb composition. We recorded a total enhancement of magnitude 1.25 eV for **across** alloying composition in the case of $AlBi_{1-x}Sb_x$. However, the energy-gap for $InBi_{1-x}Sb_x$ has experienced an improvement of 0.986 eV; increased from 0.034 eV (for InBi) to 1.02 eV (for InSb). A schematic of the increase observed in the energy band gaps

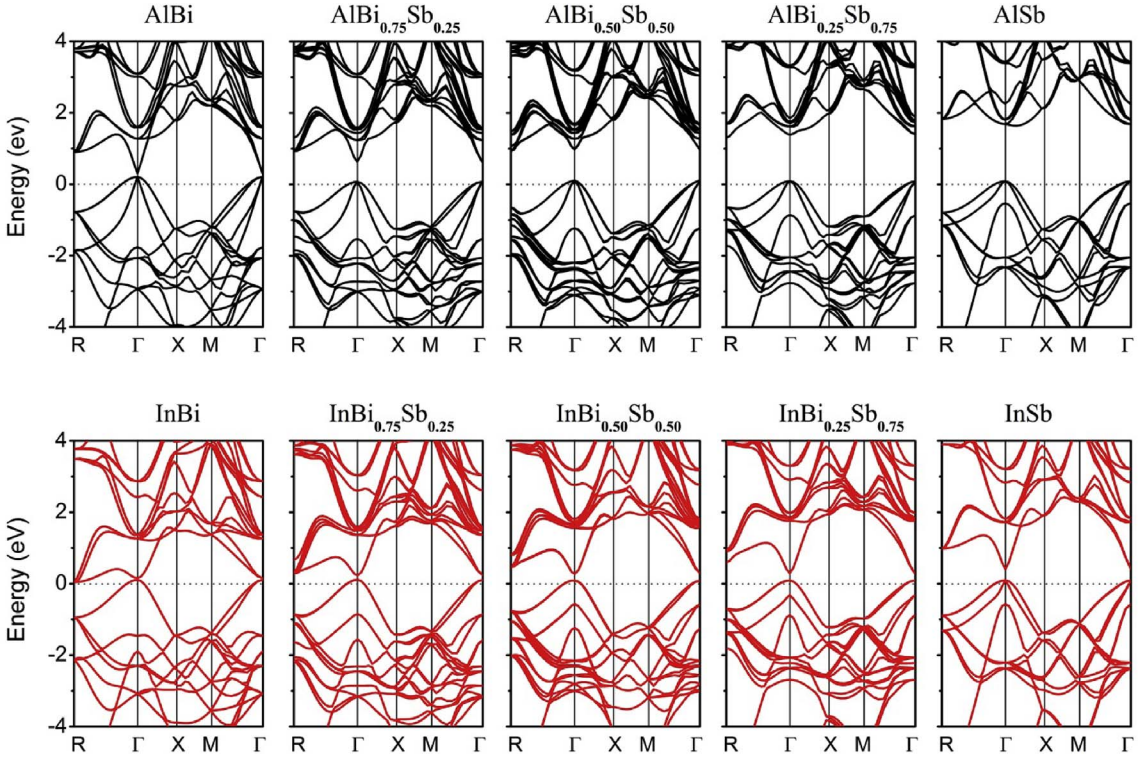

Fig. 1. The electronic band structures of $AlBi_{1-x}Sb_x$ and $InBi_{1-x}Sb_x$ for $x = 0, 0.25, 0.50, 0.75$, and 1, determined with mBJ + SOC exchange potential. The dotted line is fixed to Fermi level at 0 eV. The Sb replacement over Bi causes enhancement in the energy gap for both cases of alloys. The valence band maxima and conduction band minima occur at Γ-point for all compositions except for the AlSb. In AlSb, VBM is located at Γ-point whereas the CBM appeared along Γ-X point making it indirect bandgap material.

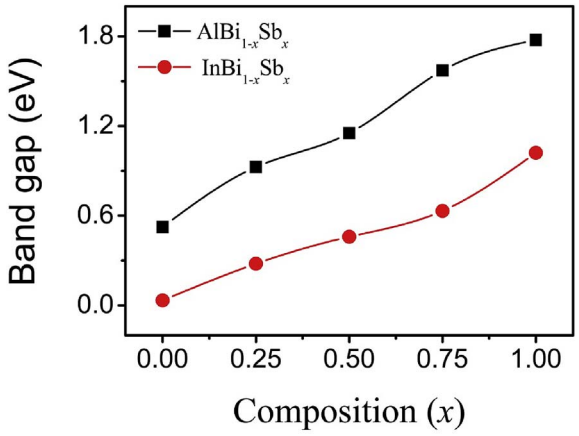

Fig. 2. The variation in the band-gap of $AlBi_{1-x}Sb_x$ and $InBi_{1-x}Sb_x$ has been shown as a function of Sb concentration. The increment of magnitude 1.25 eV and 0.986 eV has been respectively recorded in $AlBi_{1-x}Sb_x$ and $InBi_{1-x}Sb_x$for **across** composition alloying.

Table 1
The calculated energy band-gap values and effective masses of electrons in $AlBi_{1-x}Sb_x$ and $InBi_{1-x}Sb_x$ based HMAs calculated with mBJ + SOC in comparison with available values in literature.

Composition	Band Gaps (eV)		Effective mass of electrons (m_e^*/m_e)	
	This work	Other calculations	This work	Other calculations
AlBi	0.524	0.042 [39], 0.02 [40], 0.54 [43]	0.020	0.0434 [45]
$AlBi_{0.75}Sb_{0.25}$,	0.926		0.010	
$AlBi_{0.50}Sb_{0.50}$	1.152		0.004	
$AlBi_{0.25}Sb_{0.75}$	1.571		0.004	
AlSb	1.775	1.696 [41], 1.670 [39]	0.012	0.09–0.18 [39]
InBi	0.034	0.0 [39], 0.18 [43]	0.051	
$InBi_{0.75}Sb_{0.25}$,	0.279		0.010	
$InBi_{0.50}Sb_{0.50}$	0.459		0.007	
$InBi_{0.25}Sb_{0.75}$	0.632		0.004	
InSb	1.021	0.122 [42], 0.235 [41], 0.213 [39], 1.10 [44], 1.54 [44]	0.018	0.016 [46], 0.015 [41], 0.017 [44], 0.022 [44]

has been shown in Fig. 2. The energy gaps calculated for $AlBi_{1-x}Sb_x$ and $InBi_{1-x}Sb_x$ are listed and compared with results already reported in literature as shown in Table 1. It is seen that the mBJ + SOC reproduced sufficiently larger values of band-gaps than that calculated with LDA [39–41] or GGA [42], however, they are fairly comparable to that of the just mBJ [43,44] results. Table 1 shows that the energy gap values of $InBi_{1-x}Sb_x$ are comparatively narrower than that of $AlBi_{1-x}Sb_x$.

Furthermore, the substitution of Sb over Bi has shown a significant effect on the dispersion of CBM (see Fig. 1). The modifications in the dispersion of CBM are important as they describe the masses of charge carriers associated with these bands by the following equation.

$$d^2E/dk^2 = \hbar^2/m \quad (5)$$

The curvature of the CBM in both cases is strongly affected by the Sb replacement over Bi. The CBM gets flattered with an increase in Sb in the case of $AlBi_{1-x}Sb_x$, but opposite scenario was observed for $InBi_{1-x}Sb_x$ where the comparatively flatter CBM become parabolic with Sb. The effective masses of charge carriers calculated from the dispersion of the conduction band minimum over Γ-point (along Γ-X point for AlSb) are accordingly found heavier for parent compounds i. e AlBi and AlSb than in blended $AlBi_{1-x}Sb_x$ (see Table 1). Though evolution in the band dispersion of conduction band structure in case of $InBi_{1-x}Sb_x$ is less significant, the effective mass of the electrons in $InBi_{1-x}Sb_x$ are found

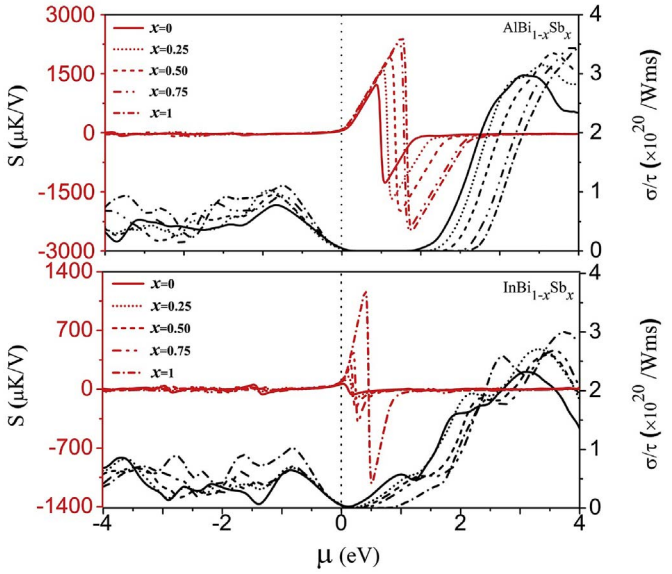

Fig. 3. Dependence Seebeck coefficient (S) (red) and electrical conductivity (σ/τ) (black) of $AlBi_{1-x}Sb_x$ and $InBi_{1-x}Sb_x$ based HMAs on Sb composition and chemical potential has been shown. Both quantities have shown a significant increase with an increase in Sb composition. The thermoelectric response of $AlBi_{1-x}Sb_x$ is recorded significantly larger than $InBi_{1-x}Sb_x$. (For interpretation of the references to colour in this figure legend, the reader is referred to the web version of this article.)

slightly decreasing as a function of Sb composition up to 75% of the alloying composition. The calculated effective masses of charge carriers are fairly comparable to the relevant available literature as well as to that of other HMAs reported in Ref. [10]. Overall, the effective masses are found comparatively heavier in $AlBi_{1-x}Sb_x$ than $InBi_{1-x}Sb_x$. Consequently, the carrier mobility is believed to be lower in $AlBi_{1-x}Sb_x$, while higher in $InBi_{1-x}Sb_x$ on account of Sb substitution over Bi. These features of the band structure/Band-gap suggest the quantitatively larger value of the thermoelectric response particularly the Seebeck coefficient value of the $AlBi_{1-x}Sb_x$ than $InBi_{1-x}Sb_x$. This effect has been accordingly reflected in Fig. 3.

Fig. 3 shows the Seebeck coefficients and electrical conductivities of $AlBi_{1-x}Sb_x$ and $InBi_{1-x}Sb_x$ against the chemical potential. The Fermi level is fixed to zero energy represented by dotted lines in Fig. 3. A negative value of chemical potential corresponds to the holes-doped region or p-type doping whereas the positive chemical potential reflects the electrons-doped region or n-type doping. The Seebeck effect takes place as a result of temperature gradient applied to a material that triggers motion in charge carriers within the medium. Such mobilized charge carriers serve as a source of heat and charge transport within inducing voltage gradient. This feature of thermoelectric materials is a principle of thermoelectric power generation. The Seebeck coefficients typically occur in the energy regime corresponding to band-gap, where the electrical conductivities approach their minimum values. Therefore, they accordingly occur in an electron-doped regime in $AlBi_{1-x}Sb_x$ and $InBi_{1-x}Sb_x$ as the band-gaps in these materials appear above Fermi level. Like the band-gaps, the Seebeck values of these materials are found sensitive to the Sb replacement over Bi and are considerably enhanced with an increase in Sb composition.

It is seen that $AlBi_{1-x}Sb_x$ based HMAs exhibit significantly large values for Seebeck coefficients that go further in the course of improvement with increase in Sb composition showing their potential application in thermoelectrics. The larger Seebeck values of $AlBi_{1-x}Sb_x$ than $InBi_{1-x}Sb_x$ are likely the result of their larger bandgaps and heavier masses of charge carrier than in $InBi_{1-x}Sb_x$.The progress observed in Seebeck values for **across** composition alloying is such that it has improved from ~82.90 μV/K (for AlBi) at Fermi-level to ~107.52 μV/K (for AlSb) at 300 K. Similarly, the Seebeck value of InBi of magnitude

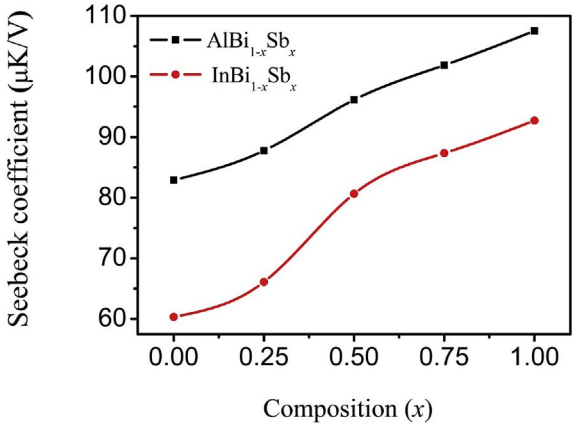

Fig. 4. Modifications in the Seebeck coefficient (S) of $AlBi_{1-x}Sb_x$ and $InBi_{1-x}Sb_x$ based HMAs on account of Sb contents over Fermi level at 300 K.

Table 2
The room temperature Seebeck coefficients (in units of μV/K) at Fermi level, the maximum electrical conductivities (σ/τ_{max} in units of 10^{20}/Ωms) with a position on energy window relative to Fermi level and ZT values of $AlBi_{1-x}Sb_x$ and $InBi_{1-x}Sb_x$ based HMAs.

Composition	S (μV/K)	Electrical conductivity		ZT
		μ (eV)	σ/τ max	
AlBi	82.90	2.31	2.97	0.988
$AlBi_{0.75}Sb_{0.25}$,	98.89	2.58	3.14	0.993
$AlBi_{0.50}Sb_{0.50}$	96.14	2.72	3.35	0.993
$AlBi_{0.25}Sb_{0.75}$	101.85	2.86	3.45	0.994
AlSb	107.52	3.13	3.47	0.998
InBi	60.32	3.13	2.32	0.132
$InBi_{0.75}Sb_{0.25}$,	66.11	3.26	2.70	0.422
$InBi_{0.50}Sb_{0.50}$	80.64	3.40	2.61	0.725
$InBi_{0.25}Sb_{0.75}$	87.35	3.54	2.67	0.874
InSb	92.73	3.67	2.97	0.982

~60.32 μV/K at Fermi-level has been increased to ~92.73 μV/K for InSb. Thus the total enhancement recorded in Seebeck value on account of **across** composition alloying magnitudes to ~25 μV/K and ~32 μV/K respectively for $AlBi_{1-x}Sb_x$ and $InBi_{1-x}Sb_x$. The improvement in Seebeck values of $InBi_{1-x}Sb_x$ is moderate up to 75% of alloying, however, it increases abruptly for InSb perhaps for its larger energy gap (Fig. 3). The course of composition induced improvement in the Seebeck values of the $AlBi_{1-x}Sb_x$ and $InBi_{1-x}Sb_x$ over Fermi level has been schematically shown in Fig. 4, and quantitatively listed in Table 2.

The temperature dependence of the Seebeck coefficients over Fermi-level has been shown in Fig. 5. It is evident that increase in temperature has triggered-up the Seebeck coefficients. The recorded increase in Seebeck values with temperature is comparatively rapid in $AlBi_{1-x}Sb_x$ than in $InBi_{1-x}Sb_x$ and is almost similar for all compositions. The improvement in Seebeck values with increase in temperature, which is rapid up to 500 K, goes modestly beyond the 500 K. This effect is more evident in the case of InBi where its Seebeck value goes still for an increase in temperature beyond the 500 K. This is likely the result of steep increase observed in the electrical conductivity above 500 K (see Fig. 6) as the two quantities hold inverse relation.

Beside Seebeck coefficients, Fig. 3 also reveals the composition dependence of electrical conductivities of $AlBi_{1-x}Sb_x$ and $InBi_{1-x}Sb_x$. The electrical conductivities are calculated with respect to relaxation time (τ) as their values depend linearly on τ within the relaxation-time approximation implemented in Boltzmann transport calculations approach. Evaluation of τ is not easy particularly in bulk materials because of several complex scattering mechanisms (carrier scattering, phonon scattering, defect scattering, and boundary scattering). In $AlBi_{1-x}Sb_x$ and $InBi_{1-x}Sb_x$ based HMAs, σ/τ is found higher for electron–doped regime as compared to holes–doped regime, which reflects the predominant n-type nature of these materials. The σ/τ of these materials shows increase with increase in Sb composition. The variation in electrical conductivity of $InBi_{1-x}Sb_x$ is however less significant compared to that of $AlBi_{1-x}Sb_x$ indeed for the relatively modest enhancement in the band-gap of $InBi_{1-x}Sb_x$. It can be seen in Fig. 3 that the increase in Sb composition lets the peaks describing the maximum value of σ/τ to shift to higher doping level on the chemical potential window. The maximum values of σ/τ and their corresponding chemical potential has been tabulated in Table 2. Our calculations for the thermoelectric properties of $AlBi_{1-x}Sb_x$ and $InBi_{1-x}Sb_x$ are in good agreement to HMAs based on GaN_xAs_{1-x} [10] and $InP_{1-x}Bi_x$ [12].

The temperature dependence of σ/τ of $AlBi_{1-x}Sb_x$ and $InBi_{1-x}Sb_x$ has been shown in Fig. 6(a and b). An exponential improvement in the σ/τ of these materials has been found with increase in temperature owing to the typical semiconducting behavior of these materials. As temperature gradient alters carrier's concentration and mobility in case of semiconductor materials that consequently evolve the electrical conductivity.

As seen in Figs. 5 and 6, the Seebeck coefficients and electrical conductivities of the $AlBi_{1-x}Sb_x$ and $InBi_{1-x}Sb_x$ exhibit nearly similar dependence on temperature i. e both the parameters increases with increase in temperature. This is an exceptional case as the two parameters hold inverse relationship in Boltzmann theory. However, the simultaneous increase in Seebeck coefficients and electrical conductivities has also been reported in several other studies [47–51]. The feature of simultaneous increase in Seebeck coefficients and electrical conductivities of these alloys make them attractive for high-temperature thermoelectric applications.

Similar to the electrical conductivities, increase in temperature has readily enhanced the thermal conductivities as shown in Fig. 6(c and d). The improvement in thermal conductivities in response to the temperature gradient can be associated with the increase in electrical

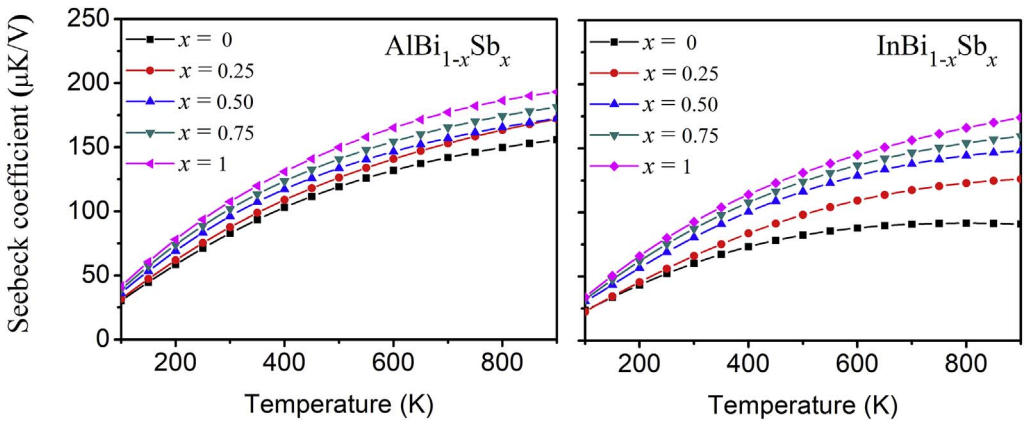

Fig. 5. Modifications in the Seebeck coefficient (S) of $AlBi_{1-x}Sb_x$ and $InBi_{1-x}Sb_x$ based HMAs over Fermi level as a function of temperature have been shown.

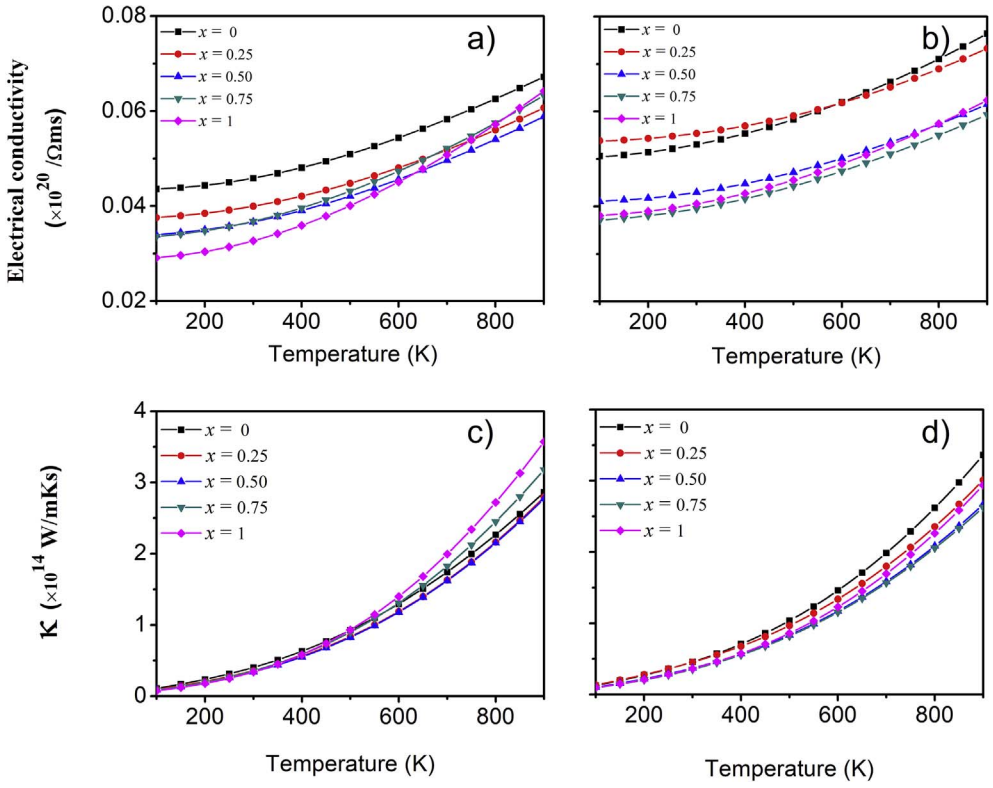

Fig. 6. Temperature dependence of electrical conductivity (σ/τ) (a,b) and thermal conductivity (κ_e/τ) (c,d) of $AlBi_{1-x}Sb_x$ and $InBi_{1-x}Sb_x$ based HMAs over Fermi-level has been shown. The course of evolution in κ_e/τ as a function of temperature has been found nearly similar to that of σ/τ because of the proportional relationship between the two quantities.

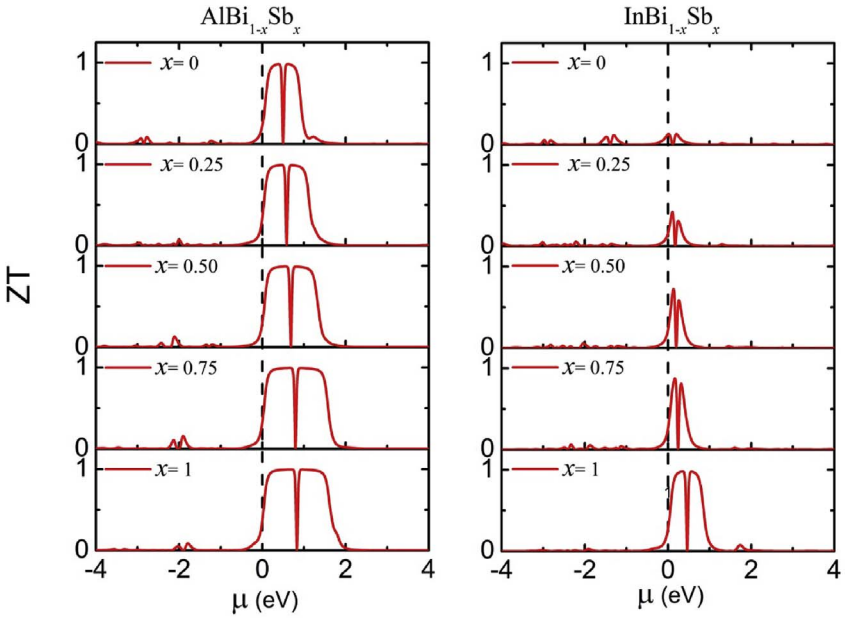

Fig. 7. The thermoelectric figure of merit (ZT) for $AlBi_{1-x}Sb_x$ and $InBi_{1-x}Sb_x$ based HMAs as a function of Sb concentration. Evidently, $AlBi_{1-x}Sb_x$ exhibit larger values of ZT than $InBi_{1-x}Sb_x$ reflecting their potential applications in thermoelectric devices.

conductivities as the two quantities hold a proportional relationship to each other. However, larger values of thermal conductivities are unwanted for thermoelectric applications as it is likely to degrade the thermoelectric figure of merit and hence the efficiency of thermoelectric materials.

The total thermal conductivity of a material is typically comprised of contribution from electrons and phonons so that $\kappa = \kappa_P + \kappa_e$. However, the BoltzTraP code used in the present study is designed such that it delivers the thermal conductivity mainly contributed from the electronic part, whereas the lattice thermal conductivity is considered to be constant as it is evident from the literature that, the increase in temperature (particularly above the room temperature) stimulates increase in thermal conductivity, which is mainly contributed by large number of the excited electrons, while the role of the lattice thermal conductivity is decreased [4] by following a relation of T^{-1} until high temperatures [52]. Therefore, the adopted Boltzmann transport theory for the calculations of thermoelectric properties has become an established approach to provide a good estimate of ZT from equation (1) [10,13,14,16].

Our calculated values of ZT have been listed in Table 2 and also schematically are shown in Fig. 7. Based on equation (1) the high value of ZT can be obtained on account of large Seebeck coefficient, higher electrical conductivity, and reduced thermal conductivity. Therefore, the tradeoff among these quantities is significant to obtain a higher

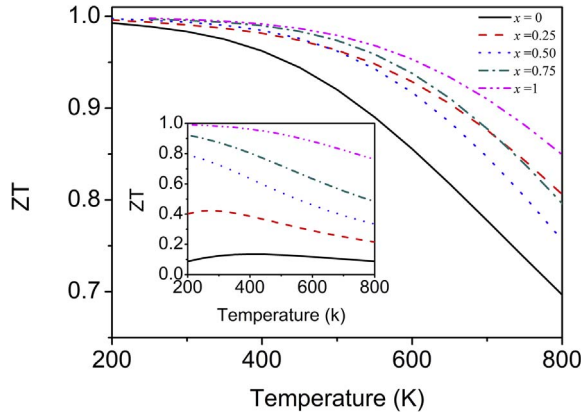

Fig. 8. The variation in thermoelectric figure of merit (ZT) of $AlBi_{1-x}Sb_x$ and $InBi_{1-x}Sb_x$ (in the inset) as a function of temperature. ZT values of $AlBi_{1-x}Sb_x$ experience significant reduction with an increase in temperature as compared to $InBi_{1-x}Sb_x$. The reduction in ZT values with increase in temperature possibly caused by increase in κ_e/τ.

value of ZT of these materials. It can be seen that $AlBi_{1-x}Sb_x$ exhibits larger ZT values for its higher values of electrical conductivity and Seebeck coefficient as compared to $InBi_{1-x}Sb_x$. It is also found that Sb replacement over Bi provokes improvement in ZT value in both types of HMAs shown in Fig. 7. The appearance of optimal Seebeck coefficients and electrical conductivities for electron-doped regions has led maximum ZT values for n-type doping.

The dependence of ZT on temperature shown in Fig. 8 reveals a decrease in ZT value with increase in temperature. The observed decrease is, however, more rapid in $AlBi_{1-x}Sb_x$ than in $InBi_{1-x}Sb_x$. This is likely reason of the less significant progression in the Seebeck coefficients of $InBi_{1-x}Sb_x$ for temperature gradient as seen in Fig. 5. Now, having established that the Seebeck coefficients and electrical conductivities of the $AlBi_{1-x}Sb_x$ and $InBi_{1-x}Sb_x$ based HMAs nurture with increase in temperature (Figs. 5 and 6(a,b)), the observed decrease in ZT is therefore solely associated with the increase in thermoelectric conductivity as seen in Fig. 6(c and d).

At the end, we present the results of thermoelectric power factors (PF) with respect to relaxation time ($S^2\sigma/\tau$) displayed in Fig. 9. It is evident that major structures in the PF are contributed either from larger seebeck coefficient, higher electrical conductivity or both. Therefore, we designate them as of type-I; contributed by larger seebeck value, type-II; stemmed from the larger electrical conductivity, and type-III; contributed simultaneously by electrical conductivity and Seebeck coefficient. Type-I structures are found to appear mainly for n-type doping at modest energies where the larger values of Seebeck coefficients for these alloys have been recorded. These structures have shown moderate intensity in the present study. Type-II structures are mainly recorded either for p-type or n-type doping corresponding to higher chemical potentials relative to Fermi level. The PFs defined by type-II structures are found to have larger values in the present study. Whereas, type-III structures are found in the vicinity of the Fermi-level where both the electrical conductivity and Seebeck coefficients exhibit considerable values. These structures are found marginal in intensity.

Table 3
The room temperature maximum PF values (in units of $10^{14}\mu W/cmK^2s$), their respective position on energy window relative to Fermi level, type of the peak describing PF_{max}, and doping type have been tabulated. The occurrence of PF_{max} at positive energy is referred to n-type doping and vice versa.

Composition	Energy	PF	Peak type	Doping-type
AlBi	1.22	7.16	II	n
$AlBi_{0.75}Sb_{0.25}$,	1.50	7.66	II	n
$AlBi_{0.50}Sb_{0.50}$	−2.04	10.28	II	p
$AlBi_{0.25}Sb_{0.75}$	−1.90	12.65	II	p
AlSb	1.77	12.32	II	n
InBi	−1.22	4.66	II	p
$InBi_{0.75}Sb_{0.25}$,	−2.18	4.25	II	p
$InBi_{0.50}Sb_{0.50}$	−2.04	4.68	II	p
$InBi_{0.25}Sb_{0.75}$	−1.90	5.23	II	p
InSb	1.77	9.59	II	n

The peaks defining the maximum values of PF for both $AlBi_{1-x}Sb_x$ and $InBi_{1-x}Sb_x$ are majorly stemmed from the electrical conductivity (Fig. 9). Table 3 shows maximum values of power factors, their corresponding energies and the type of peak that originate the PF. Since the Seebeck coefficients occur for n-type doping in all cases, the PFs appeared for p-type doping are therefore attributed to larger values of electrical conductivities at the corresponding energies. It is found that maximum PF for AlBi, $AlBi_{0.75}Sb_{0.25}$, and AlSb are of n-type as they appear for positive values of chemical potentials whereas as the PF favors p-type doping for $AlBi_{0.50}Sb_{0.50}$ and $AlBi_{0.25}Sb_{0.75}$. Similarly, InBi, $InBi_{0.75}Sb_{0.25}$, $InBi_{0.50}Sb_{0.50}$, and $InBi_{0.25}Sb_{0.75}$ exhibit their maximum PF for p-type doping, whereas InSb favors n-type doping for its maximum PF value. It is seen that the power factor results for the both

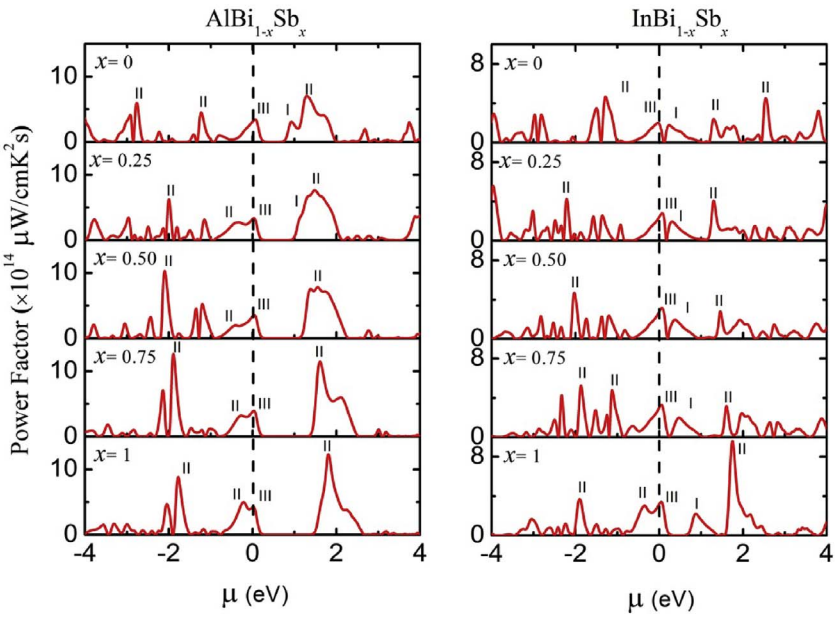

Fig. 9. The thermoelectric power factors of $AlBi_{1-x}Sb_x$ and $InBi_{1-x}Sb_x$ based HMAs determined against chemical potential have been shown. Different peaks are labeled such that type-I: contributed by larger Seebeck value, type-II: contributed by the larger value of electrical conductivity, and type-III: contributed simultaneously by electrical conductivity and Seebeck coefficient.

alloys are enhanced with an increase in Sb concentration. However, the progression of the PF is different for the both classes of alloys because of their different electronic structures. Due to the larger values of electrical conductivities and Seebeck coefficients, the thermoelectric power factors associated to $AlBi_{1-x}Sb_x$ are comparatively larger than $InBi_{1-x}Sb_x$. And so, based on the higher values of thermoelectric response, $AlBi_{1-x}Sb_x$ based HMAs are proposed as potential candidates for applications in thermoelectric devices at room temperature.

3. Conclusions

In the present DFT + Boltzmann transport theory based study, we investigated the merits of the highly mismatched alloys based on $AlBi_{1-x}Sb_x$ and $InBi_{1-x}Sb_x$ for their thermoelectric applications. The band structures of the investigated HMAs were found to be considerably evolving with the alloying composition, resulting in the enhancement of their thermoelectric response. The thermoelectric coefficients of the both classes of HMAs typically appeared for electron-doped regimes reflecting predominantly n-type nature of these materials. Similarly, the Sb-rich structures of the $AlBi_{1-x}Sb_x$ and $InBi_{1-x}Sb_x$ revealed larger values of Seebeck coefficients, the figure of merits ($\sim$1), and power factors at room temperature. However, the electrical and thermal conductivities were found greatly increasing with increasing temperature, highlighting their semiconducting nature. Although both classes of the HMAs showed evenhanded thermometric properties, the observed composition induced modifications in the $AlBi_{1-x}Sb_x$ are more noteworthy than the $InBi_{1-x}Sb_x$. Hence revealing that $AlBi_{1-x}Sb_x$ based HMAs (in particular) are believed more suitable for the conversion of heat energy into electricity at room temperature and is, therefore, looked-for further investigations particularly at the experimental level.

Acknowledgment

The authors extend their appreciation to the Deanship of Scientific Research at King Khalid University for funding this work through research groups program under grant number R.G.P. 2/3/38.

The author A. Laref acknowledges the financial support by a grant from the “Research Center of the Female Scientific and Medical Colleges”, Deanship of Scientific Research, King Saud University. F.K. Butt acknowledges the funding from Alexander von Humboldt Foundation and Federal Ministry for Education and Research (BMBF).

Appendix A. Supplementary data

Supplementary data related to this article can be found at http://dx.doi.org/10.1016/j.intermet.2017.09.017.

References

[1] A. Minnich, et al., Bulk nanostructured thermoelectric materials: current research and future prospects, Energy & Environ. Sci. 2 (5) (2009) 466–479.
[2] M. Zebarjadi, et al., Perspectives on thermoelectrics: from fundamentals to device applications, Energy & Environ. Sci. 5 (1) (2012) 5147–5162.
[3] G.J. Snyder, E.S. Toberer, Complex thermoelectric materials, Nat. Mater. 7 (2) (2008) 105–114.
[4] G. Ding, G. Gao, K. Yao, High-efficient thermoelectric materials: the case of orthorhombic IV-VI compounds, Sci. Rep. (2015) 5.
[5] D. Wang, et al., First-principles investigation of organic semiconductors for thermoelectric applications. The Journal of chemical physics, 131 (22) (2009) 224704.
[6] A.I. Hochbaum, et al., The Enhanced thermoelectric performance of rough silicon nanowires, Nature 451 (7175) (2008) 163–167.
[7] A.I. Boukai, et al., Silicon nanowires as efficient thermoelectric materials, Nature 451 (7175) (2008) 168–171.
[8] M.S. Dresselhaus, et al., New directions for low-dimensional thermoelectric materials, Adv. Mater. 19 (8) (2007) 1043–1053.
[9] J. Garg, et al., Role of disorder and anharmonicity in the thermal conductivity of silicon-germanium alloys: a first-principles study, Phys. Rev. Lett. 106 (4) (2011) 045901.
[10] A. Reshak, Thermoelectric properties of highly-mismatched alloys of GaN x as 1 − x from first-to second-principles methods: energy conversion, RSC Adv. 6 (76) (2016) 72286–72294.
[11] J.-H. Lee, J. Wu, J.C. Grossman, Enhancing the thermoelectric power factor with highly mismatched isoelectronic doping, Phys. Rev. Lett. 104 (1) (2010) 016602.
[12] S.A. Khan, S. Azam, O. Sipr, Interrelationship between structural, optical and transport properties of InP 1 − x Bix: DFT approach, Mater. Sci. Semicond. Process. 41 (2016) 45–53.
[13] B.U. Haq, et al., Composition-induced influence on the electronic band structure, optical and thermoelectric coefficients of the highly mismatched GaNSb alloy over the entire range: a DFT analysis, J. Alloys Compd. 693 (2017) 1020–1027.
[14] K. Pal, S. Anand, U.V. Waghmare, Thermoelectric properties of materials with nontrivial electronic topology, J. Mater. Chem. C 3 (46) (2015) 12130–12139.
[15] L. Müchler, et al., Topological insulators and thermoelectric materials, Phys. status solidi (RRL) Rapid Res. Lett. 7 (1–2) (2013) 91–100.
[16] T. Scheidemantel, et al., Transport coefficients from first-principles calculations, Phys. Rev. B 68 (12) (2003) 125210.
[17] G.K. Madsen, Automated search for new thermoelectric materials: the case of LiZnSb, J. Am. Chem. Soc. 128 (37) (2006) 12140–12146.
[18] J.-S. Rhyee, et al., Peierls distortion as a route to a high thermoelectric performance in In4Se3-δ crystals, Nature 459 (7249) (2009) 965–968.
[19] J. De Almeidaa, R. Ahuja, Tuning the structural, electronic, and optical properties of Be x Zn Te alloys, Appl. Phys. Lett. 89 (2006) 061913.
[20] R. Ahujaa, et al., Optical properties of SiGe alloys, J. Appl. Phys. 93 (7) (2003) 3832.
[21] B.U. Haq, et al., Study of wurtzite and zincblende GaN/InN based solar cells alloys: first-principles investigation within the improved modified Becke–Johnson potential, Sol. Energy 107 (2014) 543–552.
[22] D. Madouri, et al., Bismuth alloying in GaAs: a first-principles study, Comput. Mater. Sci. 43 (4) (2008) 818–822.
[23] H. Achour, et al., Structural and electronic properties of GaAsBi, Superlattices Microstruct. 44 (2) (2008) 223–229.
[24] N.S. Dantas, et al., Novel semiconducting materials for optoelectronic applications: Al1 − xTlxN alloys, Appl. Phys. Lett. 92 (12) (2008) 121914.
[25] F. Tran, P. Blaha, Accurate band gaps of semiconductors and insulators with a semilocal exchange-correlation potential, Phys. Rev. Lett. 102 (22) (2009) 226401.
[26] D. Koller, F. Tran, P. Blaha, Improving the modified Becke-Johnson exchange potential, Phys. Rev. B 85 (15) (2012) 155109.
[27] S. Azam, S.A. Khan, S. Goumri-Said, Modified Becke–Johnson (mBJ) exchange potential investigations of the optoelectronic structure of the quaternary diamond-like semiconductors Li 2 CdGeS 4 and Li 2 CdSnS 4, Mater. Sci. Semicond. Process. 39 (2015) 606–613.
[28] J.P. Perdew, K. Burke, M. Ernzerhof, Generalized gradient approximation made simple, Phys. Rev. Lett. 77 (18) (1996) 3865.
[29] A. MacDonald, W. Picket, D. Koelling, A linearised relativistic augmented-plane-wave method utilising approximate pure spin basis functions, J. Phys. C Solid State Phys. 13 (14) (1980) 2675.
[30] P. Novak, et al., Electronic structure of the mixed valence system (Y M) 2 BaNiO 5 (M= Ca, Sr), Phys. Rev. B 63 (23) (2001) 235114.
[31] H.J. Monkhorst, J.D. Pack, Special points for Brillouin-zone integrations, Phys. Rev. B 13 (12) (1976) 5188.
[32] P. Blaha, et al., wien2k. An Augmented Plane Wave+ Local Orbitals Program for Calculating Crystal Properties, (2001).
[33] G.K. Madsen, D.J. Singh, BoltzTraP. A code for calculating band-structure dependent quantities, Comput. Phys. Commun. 175 (1) (2006) 67–71.
[34] B.R. Nag, Electron Transport in Compound Semiconductors vol. 11, Springer Science & Business Media, 2012.
[35] B. Ul Haq, et al., Electronic structure engineering of ZnO with the modified Becke–Johnson exchange versus the classical correlation potential approaches, Phase Trans. 86 (12) (2013) 1167–1177.
[36] B.U. Haq, et al., First principles study of scandium nitride and yttrium nitride alloy system: prospective material for optoelectronics, Superlattices Microstruct. 85 (2015) 24–33.
[37] B.U. Haq, R. Ahmed, S. Goumri-Said, DFT characterization of cadmium doped zinc oxide for photovoltaic and solar cell applications, Sol. Energy Mater. Sol. Cells 130 (2014) 6–14.
[38] B.U. Haq, et al., Mutual alloying of XAs (X= Ga, In, Al) materials: tuning the optoelectronic and thermodynamic properties for solar energy applications, Sol. Energy 100 (2014) 1–8.
[39] S. Wang, H. Ye, Plane-wave pseudopotential study on mechanical and electronic properties for IV and III-V crystalline phases with zinc-blende structure, Phys. Rev. B 66 (23) (2002) 235111.
[40] B. Amrani, et al., First-principles study of AlBi, Solid State Commun. 148 (1) (2008) 59–62.
[41] I. Vurgaftman, J. Meyer, L. Ram-Mohan, Band parameters for III–V compound semiconductors and their alloys, J. Appl. Phys. 89 (11) (2001) 5815–5875.
[42] S. Namjoo, et al., Optical study of narrow bandgap InAs x Sb 1 − x (x= 0, 0.25, 0.5, 0.75, 1) alloys, Phys. Rev. B 91 (20) (2015) 205205.
[43] N.A.A. Rahim, et al., Computational modeling and characterization of X–Bi (X= B, Al, Ga, In) compounds: prospective optoelectronic materials for infrared/near infra applications, Comput. Mater. Sci. 114 (2016) 40–46.
[44] Y.-S. Kim, et al., Towards efficient band structure and effective mass calculations for III-V direct band-gap semiconductors, Phys. Rev. B 82 (20) (2010) 205212.
[45] M. Mbarki, R. Alaya, A. Rebey, Ab initio investigation of structural and electronic properties of zinc-blende AlN 1 − x Bi x alloys, Solid State Commun. 155 (2013) 12–15.
[46] R. Sladek, Effective masses of electrons in indium arsenide and indium antimonide, Phys. Rev. 105 (2) (1957) 460.
[47] P.L. Wang, et al., Decoupling the electrical conductivity and seebeck coefficient in

the RE 2SbO2 compounds through local structural perturbations, J. Am. Chem. Soc. 134 (3) (2012) 1426–1429.
[48] N. Neophytou, et al., Simultaneous increase in electrical conductivity and Seebeck coefficient in highly boron-doped nanocrystalline Si, Nanotechnology 24 (20) (2013) 205402.
[49] T. Mori, T. Nishimura, Thermoelectric properties of homologous p-and n-type boron-rich borides, J. Solid State Chem. 179 (9) (2006) 2908–2915.
[50] M.A. Hossain, et al., Crystal growth and anisotropy of high temperature thermoelectric properties of yttrium borosilicide single crystals, J. Solid State Chem. 233 (2016) 1–7.
[51] T. Mori, T. Tanaka, Effect of transition metal doping and carbon doping on thermoelectric properties of YB 66 single crystals, J. Solid State Chem. 179 (9) (2006) 2889–2894.
[52] S. Ohta, et al., High-temperature carrier transport and thermoelectric properties of heavily La-or Nb-doped Sr Ti O 3 single crystals, J. Appl. Phys. 97 (3) (2005) 034106.